ACS NANO

www.acsnano.org

ARTICLE

Persistent Exciton Dressed by Weak Polaronic Effect in Rigid and Harmonic Lattice Dion–Jacobson 2D Perovskites

Haixin Lei, Yu Xu, Yao Zhang, Qingjie Feng, Hongzhi Zhou, Wei Tang, Jiaoyang Wang, Linjun Li, Guangjun Nan, Weigao Xu, and Haiming Zhu*

Cite This: *ACS Nano* 2024, 18, 31485–31494

Read Online

ACCESS | Metrics & More | Article Recommendations | Supporting Information

ABSTRACT: The emerging two-dimensional (2D) Dion–Jacobson (DJ) perovskites with bidentate ligands have attracted significant attention due to enhanced structural stability compared with conventional Ruddlesden–Popper (RP) perovskites with monodentate ligands linked by van der Waals interactions. However, how the pure chemical bond lattice interacts with excited state excitons and its impact on the exciton nature and dynamics in 2D DJ-perovskites, particularly in comparison to RP-perovskites, remains unexplored. Herein, by a combined spectroscopy study on excitonic and structural dynamics, we reveal a persistent exciton dressed by a weak polaronic effect in DJ-perovskite due to their rigid and harmonic lattice, in striking contrast to significantly screened exciton polaron observed in RP-perovskites. Despite the similar exciton binding energy (~0.3 eV) in both n = 1 DJ- and RP-perovskites with near-identical crystal structure, photoexcitation results in a slightly screened exciton with minimal structural relaxation and a retained binding energy of ~0.29 eV in DJ-perovskites but strongly screened exciton polaron with a binding energy of ~0.13 eV in RP-perovskites. Structural dynamics further highlight the rigid and harmonic lattice motion in DJ-perovskites, as opposed to the thermally activated anharmonic lattice in RP-perovskites, arising from their distinct bonding modes. Our study offers insights into modulating excited state properties in 2D perovskites, simulating the rational design of hybrid semiconductors with tailored properties and functionalities.

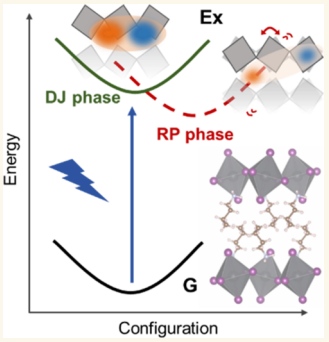

KEYWORDS: *two-dimensional DJ phase perovskites, exciton polaron, polaronic effect, spin relaxation, transient absorption spectroscopy*

Two-dimensional (2D) lead halide perovskites, characterized by alternating inorganic and organic ligand layers, have garnered substantial interest due to their tunable structures and promising applications in photonic and optoelectronic devices, such as solar cells, light-emitting diodes, and photodetectors.[1−6] Depending on the bonding type in the ligand layer, 2D perovskites can be primarily classified into two types (Figure 1A): Ruddlesden–Popper (RP) type and Dion–Jacobson (DJ) type.[4,6,7] RP-perovskites, with the general formula $(LA)_2(A)_{n-1}B_nX_{3n+1}$ where n is the inorganic layer thickness, rely on monodentate cation ligands linked by van der Waals force, while DJ-perovskites, with the formula $(LA)(A)_{n-1}B_nX_{3n+1}$, feature a single layer of bidentate cation ligand bridging the inorganic layer. The distinct bonding modes and molecular rigidity of DJ-perovskites confer them with superior structural stability, including enhanced thermal and halide ion stability, making them highly favorable for device applications.[8−15]

A prominent feature in 2D perovskites is the strongly bound electron–hole pairs, or excitons, which arise from dielectric and quantum confinement effects and manifest as sharp excitonic transitions in optical spectroscopy.[16,17] However, it is the nature and dynamics of excitons in the excited state, rather than in the ground state, that dictate the photophysical properties and performance of photoexcited semiconductors in devices. Extensive studies on 2D RP-perovskites have generally shown a complex interplay between excitons and surrounding soft, polarizable crystal lattice, promoting the formation of exciton polaron with coupled exciton-lattice dynamics.[18−25] The formation of exciton polarons has a profound impact on the properties of 2D RP-perovskites, including the excited state characteristics, exciton dissociation, radiative recombination, and spin relaxation behaviors.[18,21,26−31] A very recent preliminary study on 2D DJ-perovskite has suggested

Received: August 31, 2024
Revised: October 17, 2024
Accepted: October 23, 2024
Published: October 31, 2024

https://doi.org/10.1021/acsnano.4c12132
ACS Nano 2024, 18, 31485–31494

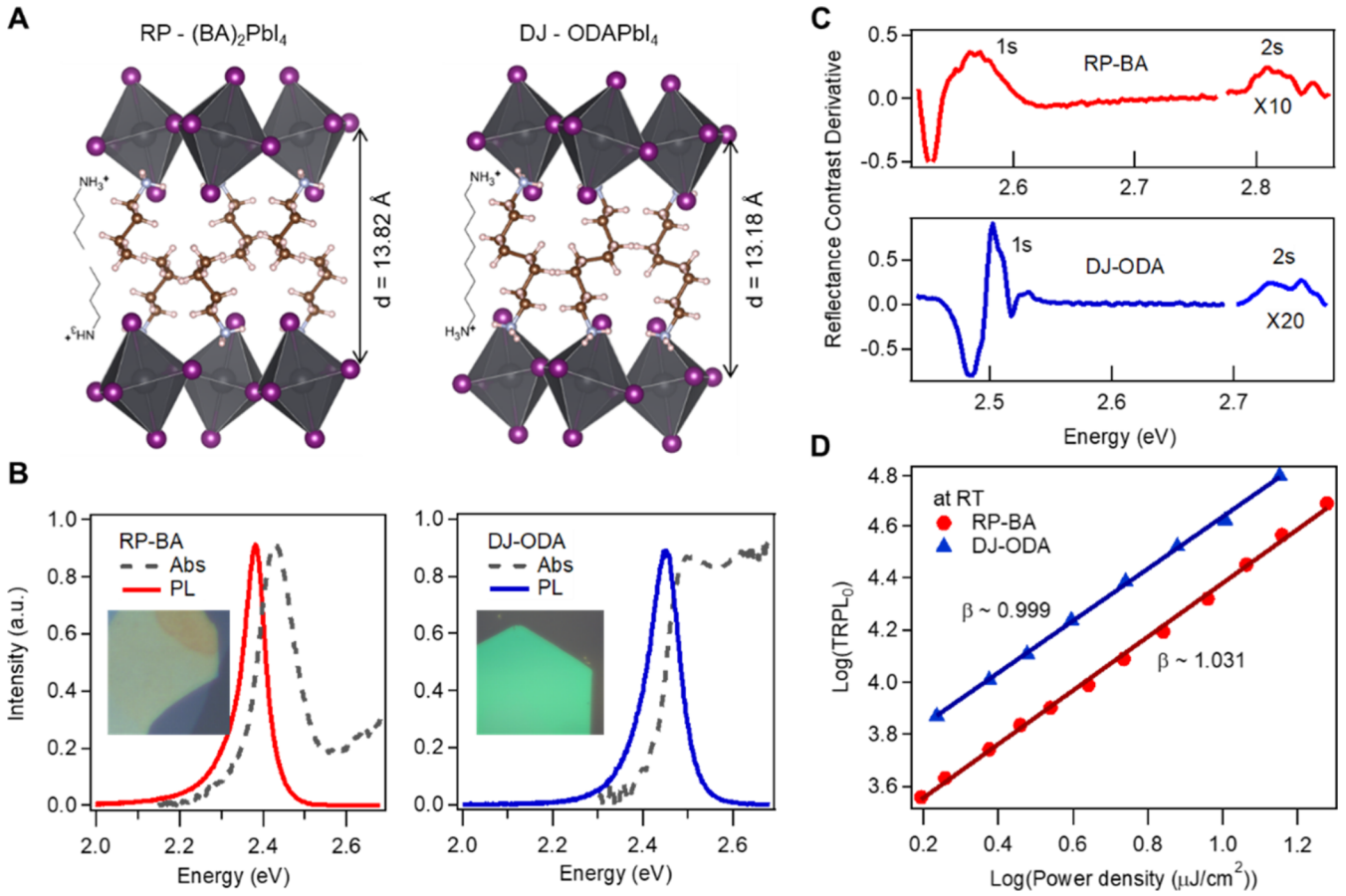

Figure 1. Crystal structure and optical characterizations. (A) Crystal and ligand structures of $(BA)_2PbI_4$ and $ODAPbI_4$. (B) The absorption and PL spectra of $(BA)_2PbI_4$ and $ODAPbI_4$ thin flakes at room temperature. Inset: optical images. (C) The derivative spectra of the reflectance contrast of $(BA)_2PbI_4$ and $ODAPbI_4$ at 4 K with denoted exciton states. (D) The log−log scale plot of $TRPL_0$ as a function of excitation power density for $(BA)_2PbI_4$ and $ODAPbI_4$ at room temperature with power β labeled.

exciton−phonon coupling and polaronic character of excitons by observing coherent phonon generation on ultrafast spectroscopy.[32] However, to what extent exciton-lattice interaction redefines the excited state exciton nature and dynamics in 2D DJ-perovskites, particularly in comparison to 2D RP-perovskites with different bonding modes, remains unexplored. This has hindered the rational design of 2D perovskite materials with tailored properties for optoelectronic applications.

In this study, we conducted combined spectroscopy studies on the electronic and structural dynamics of DJ-perovskite $ODAPbI_4$ (ODA:1,8-butanediamine) and compared it to the counterpart RP-perovskite BA_2PbI_4 (BA: *n*-butylamine) with nearly identical compositions and dielectric structures but different bonding modes. Steady-state exciton Rydberg series measurement yields a similar ground state exciton binding energy of ∼0.3 eV for both DJ-$ODAPbI_4$ and RP-BA_2PbI_4. However, the spin-resolved transient absorption spectroscopy shows opposite temperature-dependent exciton spin relaxation behavior and reveals a persistent exciton with a slightly screened binding energy of 0.29 eV in DJ-$ODAPbI_4$ but strongly screened exciton with a binding energy of 0.13 eV in RP-BA_2PbI_4 by the excited state polaronic effect. An in-depth analysis of the Stokes shift indeed reveals much less excited state structural relaxation in DJ-$ODAPbI_4$, compared with RP-BA_2PbI_4, which can be well described by the Debye dielectric relaxation model. Further study of structural dynamics by low-frequency Raman spectroscopy and theoretical calculation reveals rigid and harmonic lattice motion of DJ-$ODAPbI_4$, in striking contrast to thermally activated anharmonic lattice movement in RP-BA_2PbI_4, which originates from different ligand-bonding modes. This result indicates that despite near-identical exciton binding energy at the ground state, DJ-perovskite with bidentate ligand has a more rigid and harmonic lattice and a persistent exciton with weak polaronic effect at the excited state, compared with the contrasting RP-perovskite with monodentate ligand, soft and anharmonic lattice, and strongly screened exciton polaron. This dramatically different excited state behavior has strong implications for their optoelectronic applications.

RESULTS AND DISCUSSION

$(BA)_2PbI_4$ and $ODAPbI_4$ single crystals are synthesized using a solution growth approach (see details in Supplementary Note 1. Materials and Methods).[7,33] The obtained $(BA)_2PbI_4$ and $ODAPbI_4$ thin flakes are several hundred nanometers thick and tens of microns in lateral size (see Figure S1 atomical force microscopy images). The crystal structures were confirmed by X-ray diffraction (XRD) measurements (Figure S2). As shown in Figure 1A, $(BA)_2PbI_4$ (RP type) relies on van der Waals force to link two layers of monoammonium cation ligands with a van der Waals gap while $ODAPbI_4$ (DJ type) has only a single layer of diammonium cation ligands to conjugate the inorganic layers. For ease of terminology, $(BA)_2PbI_4$ and

https://doi.org/10.1021/acsnano.4c12132
ACS Nano 2024, 18, 31485−31494

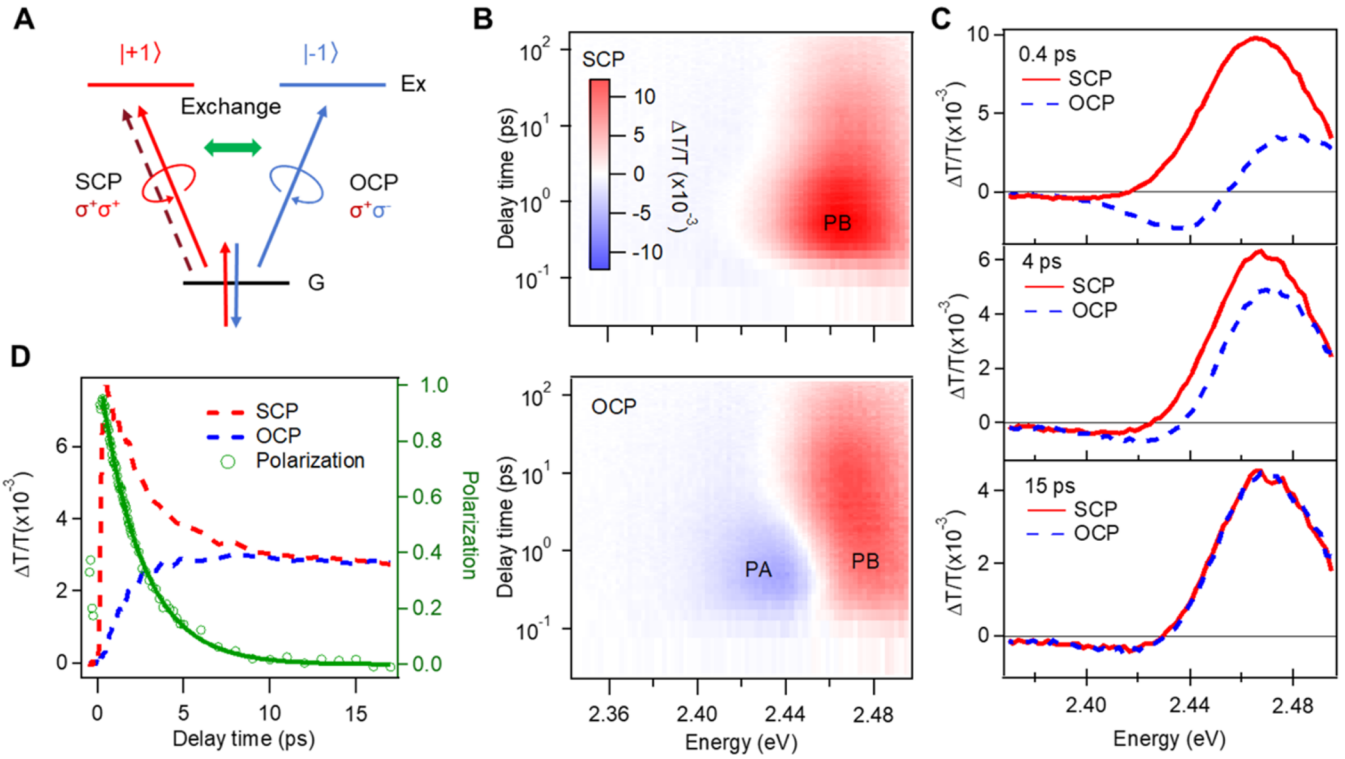

Figure 2. Spin-resolved TA spectroscopy of ODAPbI$_4$ at 280 K. (A) Scheme of spin-resolved TA measurements where spin-polarized excitons are photoexcited and probed by same (SCP) or opposite (OCP) circularly polarized light. (B) 2D color plot of TA spectra of DJ-ODA under SCP and OCP conditions. (C) Associated spectral evolution of SCP and OCP at 0.4, 4, and 15 ps, respectively. (D) SCP and OCP TA kinetics and exciton spin relaxation kinetics in DJ-ODA.

ODAPbI$_4$ are hereafter abbreviated as "RP-BA" and "DJ-ODA," respectively. Apart from the different bonding modes, their structures and compositions are highly similar, exhibiting nearly identical interlayer spacing (13.82 and 13.18 Å for RP-BA and DJ-ODA, respectively) thus dielectric structure. As shown in Figure 1B, at room temperature, RP-BA and DJ-ODA exhibit the lowest energy absorption peaks at 2.43 and 2.50 eV, respectively, and a single sharp photoluminescence (PL) peak with ∼50 meV Stokes shift, arising from their lowest energy exciton resonance.[7,33] The absence of the PL peak from other inorganic layer thicknesses or extrinsic edge states even at cryogenic temperature (Figure S3) confirms the high quality and purity of the obtained single crystals. The temperature (T)-dependent PL spectra also indicate the absence of phase transition from 80 to 320 K in RP-BA and DJ-ODA.[34,35]

We first determine the ground state exciton binding energy E_b^0 by conventional steady-state exciton Rydberg series measurement, which has been successfully applied in 2D transition-metal dichalcogenides and 2D lead halide perovskites previously.[16,36,37] We measured the reflectance contrast spectra δR of $(BA)_2PbI_4$ and ODAPbI$_4$ at 4 K and obtained reflectance contrast derivative $(d(\delta R)/dE)$ spectra which exhibit resolvable 1s/2s excitonic peaks at 2.57/2.81 eV for RP-BA and 2.50/2.73 eV for DJ-ODA, respectively (Figure 1C). Thus, E_b^0 can be estimated from the energy spacing (denoted as Δ_{12}) between 1s and 2s excitonic peaks, $E_b^0 \approx 1.35\Delta_{12}$.[16] Using this method, we obtain a nearly identical E_b^0 of 0.33 and 0.31 eV for RP-BA and DJ-ODA, respectively, which echoes their similar inorganic/organic dielectric structures. These E_b^0 values are also consistent with previous results on similar n = 1 lead iodine perovskites but with different ligands.[16,17]

Importantly, it is excited state properties, rather than ground state properties, that govern the optoelectronic performance of semiconductor materials. To have a first glance at the excited state species (excitons vs dissociated charge carriers) in these 2D perovskites, we examined the excited state radiative recombination behavior by time-resolved PL (TRPL) measurement. Specifically, the initial TRPL intensity at t = 0 (denoted as TRPL$_0$), which is proportional to the radiative recombination rate, depends on photoexcitation density linearly (i.e., TRPL$_0 \propto n_0$) for exciton monomolecular recombination and quadratically (i.e., TRPL$_0 \propto n_0^2$) for electron−hole charge bimolecular recombination.[38,39] As shown in Figure 1D, TRPL$_0$ (obtained from TRPL kinetics in Figure S4) as a function of photoexcitation density in RP-BA and DJ-ODA can be well described by TRPL$_0 \propto n_0^\beta$ with a power factor β of ∼1, confirming excitons as photoexcitation species in these n = 1 2D perovskites at room temperature.

Importantly, the ground state exciton binding energy (E_b^0) may not reflect the excited state exciton binding energy (denoted as E_b^*) if there is an excited state electronic and structural relaxation after photoexcitation.[18,22,28] Our previous study on 2D RP-lead bromide perovskite has established a method of estimating E_b^* from temperature (T)-dependent exciton spin relaxation measurements.[28] Specifically, according to the Maialle−Silva−Sham (MSS) mechanism, exciton spin relaxation in low-dimensional semiconductors is governed by the strength of electron−hole exchange interaction (J) at an excited state.[28,40−43] As J is proportional to E_b^*, E_b^*can be estimated from T-dependent exciton spin relaxation rate k_s by

$$k_s \approx \langle \Omega_K^2 \rangle \tau_p \propto J^2 T \tau_p \propto (E_b^*)^2 T/\Gamma \quad (1)$$

https://doi.org/10.1021/acsnano.4c12132
ACS Nano 2024, 18, 31485−31494

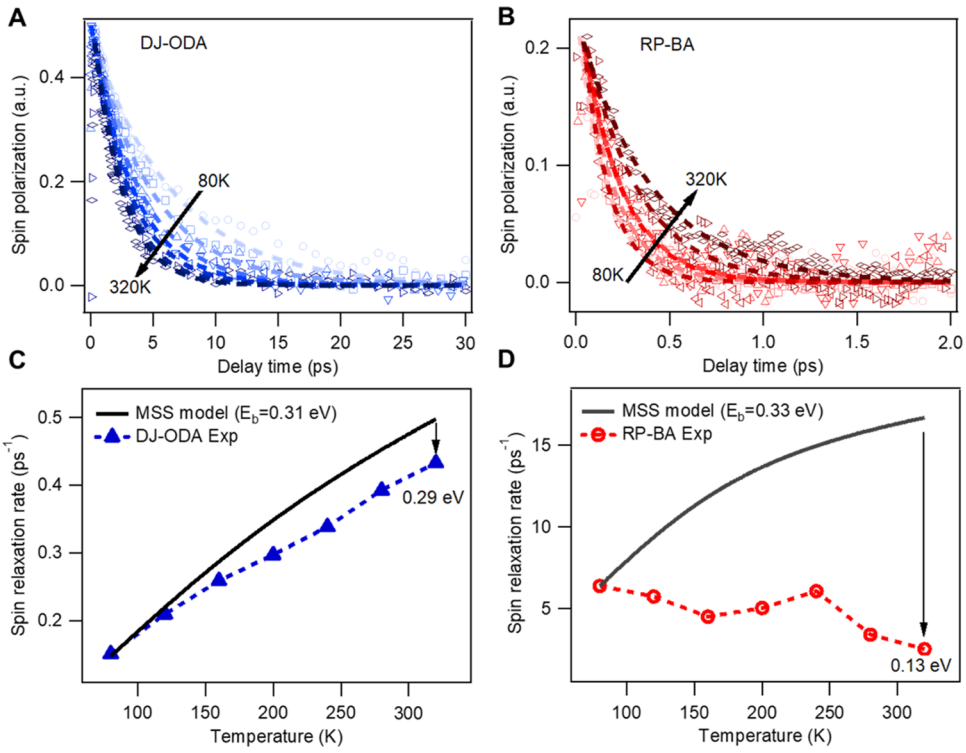

Figure 3. Temperature-dependent exciton spin relaxation. (A, B) Exciton spin relaxation kinetics with single exponential fitting at different temperatures of (A) DJ-ODA and (B) RP-BA. (C, D) Temperature-dependent exciton spin relaxation rate and the modeled results by MSS mechanism with constant $E_b = E_b^0$ for (C) DJ-ODA and (D) RP-BA.

where $\langle \Omega_K^2 \rangle$ is the square of the effective magnetic field, which depends on the electron−hole interaction, τ_P is the exciton scattering time, which is inversely proportional to PL line width Γ, and T is the temperature. The MSS mechanism has well described the T-dependent exciton spin relaxation in conventional quantum wells and 2D transition-metal dichalcogenides.[28,40−42]

To determine the exciton spin-flip rate, we performed spin-resolved femtosecond transient absorption (TA) spectroscopy on DJ-ODA and RP-BA from 80 to 320 K. As shown schematically in Figure 2A, we photoexcite spin-polarized excitons $|+1\rangle$ (or $|-1\rangle$) by circularly polarized σ^+ (or σ^-) pump pulse and subsequently measure exciton population using another circularly polarized probe pulse with the same circular polarization (SCP) or opposite circular polarization (OCP).[18,28,44−48] Generally, the TA signal in 2D semiconductors originates from the combined band-filling effect and Coulombic effect (e.g., band renormalization, exciton screening).[28,44,46] While the Coulombic effect would apply to both exciton spin states, which will not produce spectral difference between SCP and OCP, the band-filling effect is sensitive to photogenerated exciton occupation in a specific spin state, generating spectral difference between SCP and OCP.

The spin-resolved TA results of DJ-ODA at near-resonant (2.51 eV) excitation under SCP and OCP conditions are shown in Figure 2B, with representative TA spectra at different delay times (0.4, 4, and 15 ps) shown in Figure 2C. The pump fluence was kept low enough to ensure the TA signal in a linear regime. Right after photoexcitation (e.g., 0.4 ps), the OCP spectra exhibit a derivative line shape with positive photoinduced absorption (PA) and negative photoinduced bleach (PB) features around exciton resonance, which can be ascribed to spin-independent Coulomb effect. On the other hand, the SCP spectra show a dominant PB feature at exciton resonance due to combined band-filling and Coulomb effect. The spectral difference between SCP and OCP represents the exciton spin polarization in DJ-ODA and disappears at about 10 ps, indicating a fast spin relaxation process.[28,44,46−49] The degree of exciton spin polarization (Pol) can be calculated by $\mathrm{Pol}(t) = \frac{\mathrm{TA_{SCP}} - \mathrm{TA_{OCP}}}{\mathrm{TA_{SCP}} + \mathrm{TA_{OCP}}}$. As shown in Figure 2D, the exciton spin polarization in DJ-ODA exhibits a rapid decay at room temperature with a lifetime of 2.58 ± 0.04 ps by single exponential decay fitting. As a comparison, we also performed similar spin-dependent TA measurements on RP-BA and the results are shown in Figure S7. The spin relaxation rates were found to increase slightly with the increase of photoexcitation density in both RP- and DJ-perovskites.[30,48] At the same time, a narrow and sharp PL spectrum at liquid nitrogen temperature without carrier doping feature (Figure S3) and absent second-harmonic generation (SHG) signal (Figure S5) further prove the dominant MSS spin relaxation mechanism rather than the Bir−Aronov−Pikus (BAP) or the D'yakonov-Perel (DP) mechanism.

To determine E_b* according to eq 1, we measured T-dependent exciton spin relaxation in DJ-ODA (Figure S6) and RP-BA (Figure S7) between 80 and 320 K.[28] The exciton spin relaxation kinetics at different temperatures for DJ-ODA and RP-BA are shown in Figure 3A,B, respectively. Interestingly, with increasing temperature, exciton spin relaxation is accelerated in DJ-ODA and decelerated in RP-BA. The k_s values by single exponential decay fitting are plotted in Figure 3C,D for $ODAPbI_4$ and $(BA)_2PbI_4$, respectively, showing interestingly opposite temperature dependence behavior.

https://doi.org/10.1021/acsnano.4c12132
ACS Nano 2024, 18, 31485−31494

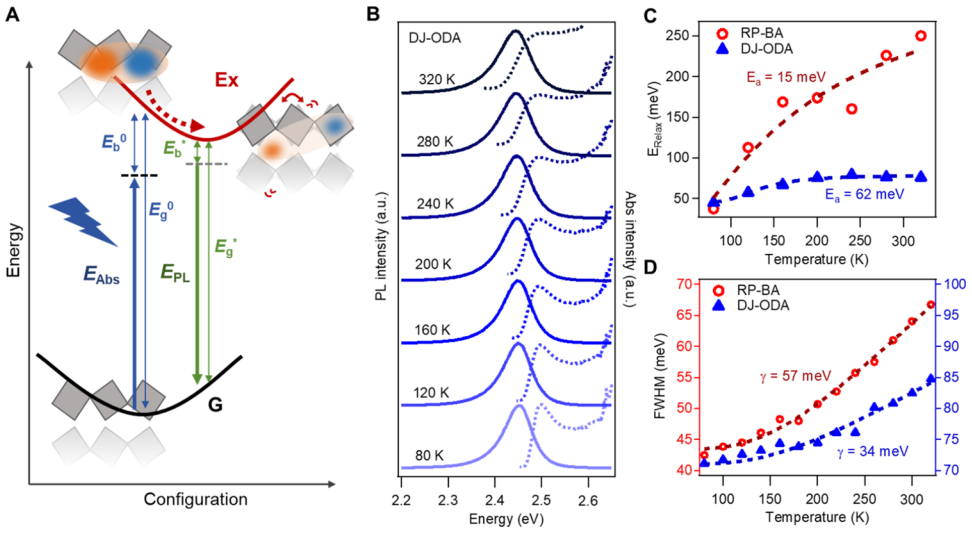

Figure 4. Excited state relaxation by exciton−phonon coupling. (A) Scheme of excited state relaxation and associated energetics including optical transition energy and exciton binding energy. (B) Absorption and PL spectra of DJ-ODA at different temperatures. (C) Relaxation energy as a function of the temperature and the fits (dashed lines) by the Debye relaxation model. (D) PL fwhm as a function of the temperature and the fits (dashed lines).

As RP-BA and DJ-ODA both exhibit strong exciton recombination at RT (Figure 1D), we measured that they still maintain high exciton binding energy after high-temperature screening, and their spin relaxation is still dominated by exchange interactions. Thus, we inferred that the MSS mechanism is still valid to apply the model to extract E_b* values for both perovskites. With Γ from *T*-dependent PL spectra (Figure S3) and assuming a constant E_b*, we modeled the *T*-dependent k_s for DJ-ODA and RP-BA by eq 1. The modeled k_s curve has been scaled to match the experimental value at 80 K where large amplitude lattice motion is mostly frozen and excited state polaronic effect is negligible (i.e., E_b* = E_b^0).[50] As shown by the black line in Figure 3C,D, the modeled k_s in both systems increases with increasing temperature, consistent with *T*-dependent behavior in 2D quantum wells and transition-metal dichalcogenides.[28,40−42] Interestingly, the measured k_s in DJ-ODA agrees well with the modeled curve except for a slight deviation at high temperature, while the measured and modeled k_s in RP-BA show a completely opposite trend.

According to eq 1, the negative deviation of the experimental k_s compared with the modeled value indicates screened E_b* (relative to E_b^0) in these 2D perovskites at higher temperatures. Since spin relaxation is an excited state behavior rather than ground state behavior, the screened E_b* is the excited state exciton binding energy described in eq 1. The nice agreement with a slight deviation in DJ-ODA but the opposite trend in RP-BA indicates a persistent exciton with mostly retained E_b* in the former but significantly screened E_b* in the latter at room temperature. Since $k_s \propto (E_b^*)^2$, E_b* can be quantitatively calculated by the extent of deviation between measured and model k_s according to eq 1 (see SI Note 2).[18,28] For example, for RP-BA at 320 K, the measured k_s is 6.62 times smaller than the modeled value, from which we can obtain a screened E_b* of ∼0.13 eV. As a contrast, we obtain a much larger E_b* ∼ 0.29 eV for DJ-ODA at the same temperature, despite the similar E_b^0 ∼ 0.3 eV for DJ-ODA and RP-BA.

Because of their polar, anharmonic, and dynamic lattice, metal halide perovskites exhibit a liquid-like dielectric response thus excitons in 2D perovskites after photoexcitation can polarize the surrounding crystal lattice through exciton−phonon coupling (i.e., polaronic effect), forming stabilized exciton polarons with localized electronic wave function and distorted lattice (Figure 4A).[18−23,25,26,28,50−53] The excited state relaxation to the exciton polaron by the polaronic effect after vertical photoexcitation in 2D perovskite is in analogy to the solvation process in liquids. Because oppositely charged electron and hole mutually deform the polar lattice in the opposite way, the formation of exciton polaron would weaken the electron−hole Coulomb interaction, leading to a screened E_b*.[28] Compared with RP-BA showing significantly screened E_b* at room temperature, the retained E_b* in DJ-ODA indicates much weaker excited state structural relaxation and exciton−phonon coupling in DJ-ODA. According to the extent of E_b* screening (relative to E_b^0), the local effective dielectric constant is increased by 6.8% in DJ-ODA and 153.8% in RP-BA after forming exciton polaron with lattice distortion.

The excited state relaxation by the liquid-like dielectric response can be inferred from *T*-dependent stokes shift as the associated large amplitude and anharmonic structural relaxation is nearly frozen in cryogenic temperature and activated at high temperature.[50,54,55] By comparing absorption and PL spectra at different temperatures (80−320 K) (Figure 4B for DJ-ODA and Figure S8 for RP-BA), we extracted the *T*-dependent stokes shift (E_{Stokes}). As shown in Figure S9, with increasing temperature from 80 to 320 K, E_{Stokes} of DJ-ODA is increased by ∼6.6 meV, half of that (∼13 meV) in RP-BA. In 3D semiconductors where the excitonic effect is negligible, E_{Stokes} directly reflects the pure electronic structure relaxation energy (E_{Relax}) on the potential energy surface after vertical photoexcitation.[50,56] However, in 2D semiconductors with screened E_b*, the excitonic effect must be considered to account for the exciton binding energy change. As shown in Figure 4A, the energy of absorption and PL in 2D excitonic systems can be given by $E_{Abs} = E_g^0 - E_b^0$ and $E_{PL} = E_g^* - E_b^*$, respectively, where E_g^0 and E_g^* are the vertical transition energy on the potential energy surface at the ground state and excited state equilibrium configuration, respectively. Therefore,

https://doi.org/10.1021/acsnano.4c12132
ACS Nano 2024, 18, 31485−31494

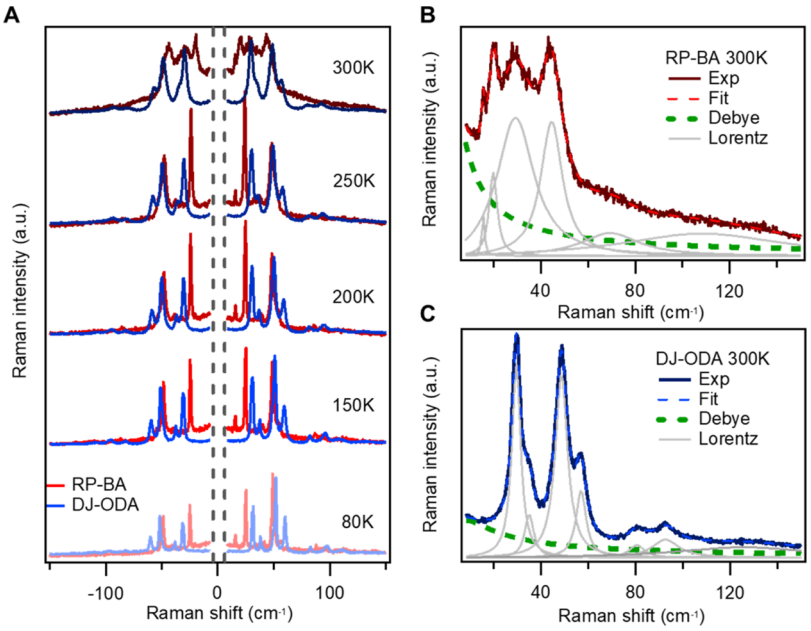

Figure 5. Temperature-dependent low-frequency Raman spectra. (A) Low-frequency Raman spectra of DJ-ODA (blue) and RP-BA (red) at 80−300 K. (B, C) Measured and fitted low-frequency Raman spectra of (B) RP-BA and (C) DJ-ODA at 300 K. Gray and green lines are the Lorentz oscillator components and Debye components, respectively.

E_{Relax} on the potential energy surface in 2D systems can be given by $E_{Relax} = E_g^0 - E_g^* = E_{Stokes} + E_b^0 - E_b^*$, which contains both the Stokes shift and the exciton binding energy change. E_b^0 and E_b^* have been obtained from exciton Rydberg series measurement and T-dependent spin relaxation measurement above, respectively, which, together with E_{Stokes}, yield E_{Relax} at different temperatures. As shown in Figure 4C, with increasing temperature from 80 to 320 K, E_{Relax} in DJ-ODA is increased by 31 meV, about 1 order of magnitude smaller than that (~215 meV) in RP-BA. As a comparison, the E_{Relax} we determined in DJ-ODA here is close to the recently calculated excited state reorganization energy (~50 meV) in DJ-type (FPP)PbI_4 (FPP: 2-fluoro-[1,1′-biphenyl]-4,4′-diyl)-dimethanaminium).[32] The much smaller increment of E_{Relax} in DJ-ODA confirms little excited state structural relaxation, in agreement with much less excited state polaronic screening effect and persistent exciton with retained E_b^* in DJ-ODA.

According to the dielectric continuum solvation model (Debye relaxation) or solid state polaron theory, E_{Relax} depends on the difference between static (ε_0) and high frequency (ε_∞) dielectric constant by $E_{Relax} \propto \left(\frac{1}{\varepsilon_\infty} - \frac{1}{\varepsilon_0}\right)$ and the T-dependent E_{Relax} originates from T-dependent ε_0.[50,56] Specifically, at low temperature, the liquid-like large amplitude and anharmonic nuclear displacement (e.g., rotation, reorientation) are nearly frozen and lattice motion is mostly harmonic; thus, ε_0 is nearly identical to ε_∞, leading to a small E_{Relax} while at high temperatures, such nuclear displacement is facile and lattice motion can sample the anharmonic potential energy surface, inducing a large increase in ε_0 and E_{Relax}. According to the Debye relaxation model, the thermally activated ε_0 can be approximately described by $\varepsilon_0 = \varepsilon_\infty + \frac{A}{\exp\left(\frac{E_a}{kT}\right) - 1}$, where A is a prefactor and E_a is an effective thermal activation energy for accessing anharmonic lattice motion.[50] As shown in Figure 4C, we fit the T-dependent E_{Relax} by this relaxation model and obtained an E_a of 62 and 15 meV for DJ-ODA and RP-BA, respectively. The much larger E_a indicates that the lattice of DJ-ODA is much more rigid and harmonic than that of RP-BA, leading to persistent exciton dressed by a weak polaronic effect at the excited state.

The weaker excited state polaronic effect in DJ-ODA can also be inferred by analyzing the T-dependent PL spectral line width, which contains information on exciton−phonon coupling.[18,50,57,58] We extracted the full width at half-maximum (fwhm) of PL spectra at different temperatures (80−320 K) for RP-BA and DJ-ODA and they both increase with temperature, with a larger increase for RP-BA (Figure 4D). The T-dependent fwhm of PL spectra can be phenomenologically described by $\mathrm{FWHM}(T) = \Gamma_0 + \frac{\gamma}{[\exp(E_{ph}/k_BT - 1)]}$, where Γ_0 is the T-independent line width contribution, E_{ph} is the effective phonon energy, and γ is the exciton−phonon coupling strength. By fitting the T-dependent fwhm of PL spectra (Figure 4D), we obtain a coupling strength γ = 34 meV for DJ-ODA and 57 meV for RP-BA, confirming weaker exciton−phonon coupling in the former and stronger in the latter.

To unravel the different structural dynamics in DJ-ODA and RP-BA, we performed T-dependent low-frequency Raman spectra measurements which are sensitive to lattice disorder and anharmonicity.[59−62] The low-frequency Raman spectra of DJ-ODA and RP-BA from 80 to 300 K are compared in Figure 5A. At low temperatures (e.g., 80 K), both DJ-ODA and RP-BA exhibit sharp Raman peaks, indicating harmonic lattice motion at low temperatures. As temperature increases, these Raman peaks shift and broaden, and more importantly, a broad central peak emerges, especially in RP-BA. As shown in Figure 5B,C, at 300 K, RP-BA exhibits an obvious broad central peak superimposed by several diffusive peaks while the Raman peaks of DJ-ODA are still narrow. Such central peak features in Raman spectra have been observed in solvent liquids and 3D/2D perovskites and attributed to thermally activated anharmonic lattice motion with weak restoring force, e.g.,

https://doi.org/10.1021/acsnano.4c12132
ACS Nano 2024, 18, 31485−31494

molecular rotation in liquids and octahedral tilting/rotation in perovskites.[59−61,63−65]

To show the central peak more clearly, we performed a multipeak fitting on Raman spectra by a combination of a Debye relaxation component associated with the central peak and multiple harmonic Lorentz oscillator components associated with narrow Raman peaks (see SI Note 3).[59,60,62] As shown in Figure 5B,C (300 K) and Figure S10 (80−300 K), with increasing temperature from 80 K, RP-BA quickly exhibits a large portion of Debye central peak components compared with DJ-ODA, which does not show Debye component until 200 K, confirming a more rigid and harmonic lattice of DJ-ODA. The low-frequency Raman result is consistent with the observed E_b* and smaller E_{Relax} by weak excited state polaronic effect in DJ-ODA, in striking contrast to RP-BA.

The dramatically different excited state electronic and structural dynamics between DJ and RP perovskites ultimately originates from their different bonding mode in the ligand layer, i.e., monolayer ligand with a pure chemical bond in DJ-perovskite and bilayer ligand with van der Waals force binding in RP-perovskite. We calculated the orientation-dependent Young's modulus of DJ-ODA and RP-BA to compare their lattice stiffness quantitatively (see SI Note 4). As shown in Figure S11, Young's modulus of DJ-ODA and RP-BA differ very little in the in-plane (001) direction but significantly in the out-plane (100) and (010) directions. Specifically, along the direction of the ligand axis projected onto the (100) and (010) plane, DJ-ODA is ∼35% and ∼45% larger than RP-BA, respectively, revealing the dominant contribution of molecular rigidity in the ligand layer. The larger Young's modulus in DJ-ODA confirms a more stiffened and less deformable lattice in DJ-perovskites than the counterpart RP-perovskites originating from different ligand- binding modes, which is consistent with previous studies on the structural stability of DJ- and RP-perovskites.[8−14]

Combining the results above, it is interesting and significant that different bonding modes in the ligand layer of 2D perovskite lead to a huge difference in their excited state properties. The highly similar crystal and dielectric structures of DJ-ODA and RP-BA lead to near-identical E_b^0 ∼ 0.3 eV at the ground state. However, DJ-perovskite with bidentate ligand has a more rigid and harmonic lattice and weaker exciton−phonon coupling, thus exhibits a much smaller structural relaxation (E_{Relax}) after photoexcitation and a retained E_b* ∼ 0.29 eV by weak polaronic effect while the counterpart RP-perovskite with monodentate ligand has a softer and anharmonic lattice and stronger exciton−phonon coupling, thus a larger E_{Relax} and a significantly screened E_b* ∼ 0.13 eV. To demonstrate the persistent exciton with weak polaronic effect is general in DJ-perovskites, we performed T-dependent exciton spin relaxation measurements on another DJ-perovskite with 1,4-butanediamine (BDA) ligand $BDAPbI_4$, which exhibits similar excited state exciton behavior with retained E_b* as $ODAPbI_4$ (Figure S12). Interestingly, a very recent ultrafast spectroscopy study also shows the polaronic character of excitons in DJ-type perovskites by observing coherent phonon generation.[32] Liu et al. reported the ultrafast lattice deformation and polaron state formation in RP-type perovskites, which caused by the motion of organic molecules drives the deformation of inorganic framework.[66] Another very recent ultrafast exciton propagation study notes that ligand anchoring in RP-type perovskites can significantly improve lattice rigidity and reduce disorder to enhance exciton mobility.[67] Here, by careful comparison of DJ- and RP-perovskites with near-identical compositions and dielectric structure but only different bonding modes, we show that the excited state polaronic effect is much weaker and has little effect on exciton nature and dynamics in DJ-perovskites, compared with the counterpart RP-perovskites.

Importantly, rather than E_b^0, E_b* governs the photophysical and optoelectronic properties of 2D perovskites and has strong implications for their optoelectronic applications. Persistent exciton with little excited state structure relaxation and retained E_b* in DJ-perovskites means a faster exciton monomolecular radiative recombination with smaller PL line width, which are beneficial for the high efficiency and color purity light emission applications, e.g., lasers and light-emitting devices. As a contrast, exciton polaron with strong structural relaxation and significantly screened E_b* in RP-perovskites suggests a high-efficiency internal exciton dissociation, which is essential for charge separation-based applications such as solar cells and photodetectors.[4] For the n = 1 perovskites above, because the screened E_b* ∼ 0.13 eV in RP-BA (n = 1) is still much larger than k_BT, RP-BA (n = 1) still exhibits excitonic recombination behavior as revealed by β ∼ 1 on $TRPL_0$ measurements, same as DJ-ODA (n = 1) (Figure 1D). We have also compared the excited state species and recombination behavior in n = 2 and n = 3 DJ-ODA and RP-BA perovskites by $TRPL_0$ measurements (Figure S13S). For n = 2 where the exciton binding energy is smaller than n = 1, the power factor β is ∼1.09 in DJ-ODA (n = 2) and 1.51 in RP-BA (n = 2), confirming persistent excitons in the former but a substantial fraction of electron/hole charge carriers in later, which can be attributed to a smaller polaronic screening effect in the former than in later. By further increasing n = 3, the power factor β increases to 1.50 and 1.65 for DJ-ODA (n = 3) and RP-BA (n = 3), respectively, because of an even smaller exciton binding energy at n = 3. But still, a larger fraction of excitons is retained in DJ-ODA than in RP-BA because of the smaller excited state polaronic effect. Therefore, from a practical point of view, RP phase perovskites are favored for charge transfer applications, while DJ phase perovskites are for light emission applications.

CONCLUSIONS

In conclusion, we have performed a combined spectroscopy study on excitonic and structural dynamics in 2D DJ-perovskites by comparing them to the corresponding RP-perovskites with nearly identical composition and dielectric structure, revealing the significant excited state behaviors due to distinct bonding modes. Although steady-state exciton Rydberg series measurement indicates a similar ground state E_b^0 of ∼0.3 eV in both 2D perovskites, DJ-$ODAPbI_4$ shows a persistent exciton with retained E_b* of 0.29 eV by weak polaronic effect while RP-BA_2PbI_4 shows strongly screened exciton polaron with E_b* of 0.13 eV. An in-depth analysis of the Stokes shift confirms much less excited state structural relaxation in DJ-$ODAPbI_4$ compared with RP-$(BA)_2PbI_4$, which can be well described by the Debye dielectric relaxation model. Further structural dynamics study by low-frequency Raman spectroscopy reveals a rigid and harmonic lattice of DJ-$ODAPbI_4$, in striking contrast to thermally activated anharmonic lattice motion in RP-BA_2PbI_4, which originates from different ligand-bonding modes. The persistent exciton with retained E_b* in DJ-perovskites leads to robust excitonic radiative recombination, which is beneficial for light emission

https://doi.org/10.1021/acsnano.4c12132
ACS Nano 2024, 18, 31485−31494

applications while the exciton polaron with significantly screened E_b* thus large fraction of dissociated charge carriers in RP-perovskites is favored for charge transfer applications. Our study elucidates the excited state exciton and structural dynamics of DJ-perovskites, highlights the critical role of the ligand-bonding mode, and provides a foundation for the rational design of hybrid semiconductors with tailed excited state properties and functionalities.

METHODS/EXPERIMENTAL

The details of experimental methods are provided in Supplementary Note 1. Briefly speaking, the preparation of $(BA)_2PbI_4$, $ODAPbI_4$, and $BDAPbI_4$ single crystal process involves dissolving precursors in HI and H_3PO_2 solutions, heating to specific temperatures, and allowing the solution to cool to room temperature for crystal precipitation. The resulting crystals are then isolated, washed, and dried under a vacuum. Femtosecond transient absorption (TA) measurements were conducted using a custom microscope setup with a cryostat, a Yb:KGW laser, and a motorized delay stage to control the pump−probe delay with the TA signal calculated by normalizing the probe spectra and polarization states manipulated using wave plates. We performed ultralow-frequency Raman spectral measurements using a confocal micro-Raman spectrometer with a CCD, a 50× objective lens, and a 633 nm laser, employing BragGrate notch filters for plasma line removal and a cryostat for temperature control.

ASSOCIATED CONTENT

Supporting Information

The Supporting Information is available free of charge at https://pubs.acs.org/doi/10.1021/acsnano.4c12132.

Complete materials and experimental details; additional TA, PL, and Raman results at different temperatures; computational details and analysis (PDF)

AUTHOR INFORMATION

Corresponding Author

Haiming Zhu − *State Key Laboratory of Modern Optical Instrument, Zhejiang Key Laboratory of Excited-State Energy Conversion and Energy Storage, Department of Chemistry, Zhejiang University, Hangzhou, Zhejiang 310027, China; ZJU-Hangzhou Global Scientific and Technological Innovation Center, Hangzhou, Zhejiang 311200, China;* orcid.org/0000-0001-7747-9054; Email: hmzhu@zju.edu.cn

Authors

Haixin Lei − *State Key Laboratory of Modern Optical Instrument, Zhejiang Key Laboratory of Excited-State Energy Conversion and Energy Storage, Department of Chemistry, Zhejiang University, Hangzhou, Zhejiang 310027, China; ZJU-Hangzhou Global Scientific and Technological Innovation Center, Hangzhou, Zhejiang 311200, China*

Yu Xu − *Key Laboratory of Mesoscopic Chemistry, School of Chemistry and Chemical Engineering, Nanjing University, Nanjing, Jiangsu 210023, China*

Yao Zhang − *State Key Laboratory of Modern Optical Instrument, Zhejiang Key Laboratory of Excited-State Energy Conversion and Energy Storage, Department of Chemistry, Zhejiang University, Hangzhou, Zhejiang 310027, China; ZJU-Hangzhou Global Scientific and Technological Innovation Center, Hangzhou, Zhejiang 311200, China*

Qingjie Feng − *Department of Physics, Zhejiang Normal University, Jinhua, Zhejiang 321004, China*

Hongzhi Zhou − *State Key Laboratory of Modern Optical Instrument, Zhejiang Key Laboratory of Excited-State Energy Conversion and Energy Storage, Department of Chemistry, Zhejiang University, Hangzhou, Zhejiang 310027, China; ZJU-Hangzhou Global Scientific and Technological Innovation Center, Hangzhou, Zhejiang 311200, China;* orcid.org/0000-0001-6947-9265

Wei Tang − *State Key Laboratory of Extreme Photonics and Instrumentation, College of Optical Science and Engineering, Zhejiang University, Hangzhou 310027, China*

Jiaoyang Wang − *State Key Laboratory of Modern Optical Instrument, Zhejiang Key Laboratory of Excited-State Energy Conversion and Energy Storage, Department of Chemistry, Zhejiang University, Hangzhou, Zhejiang 310027, China; ZJU-Hangzhou Global Scientific and Technological Innovation Center, Hangzhou, Zhejiang 311200, China*

Linjun Li − *State Key Laboratory of Extreme Photonics and Instrumentation, College of Optical Science and Engineering, Zhejiang University, Hangzhou 310027, China;* orcid.org/0000-0002-2734-0414

Guangjun Nan − *Department of Physics, Zhejiang Normal University, Jinhua, Zhejiang 321004, China;* orcid.org/0000-0002-5185-8336

Weigao Xu − *Key Laboratory of Mesoscopic Chemistry, School of Chemistry and Chemical Engineering, Nanjing University, Nanjing, Jiangsu 210023, China;* orcid.org/0000-0002-3014-756X

Complete contact information is available at: https://pubs.acs.org/10.1021/acsnano.4c12132

Notes

The authors declare no competing financial interest.

ACKNOWLEDGMENTS

H. Zhu acknowledges the National Natural Science Foundation of China (22273084) and the Department of Science and Technology of Zhejiang Province (2024C01191). W. Xu acknowledges the National Natural Science Foundation of China (22333004). G. Nan acknowledges the National Natural Science Foundation of China (22273088), the Hefei National Research Center for Physical Sciences at the Microscale (KF2021004), and the Scientific Research Fund of Zhejiang Provincial Education Department (Y202250336). This work was supported by the open fund of the state key laboratory of molecular reaction dynamics in DICP, CAS.

REFERENCES

(1) Azmi, R.; Utomo, D. S.; Vishal, B.; Zhumagali, S.; Dally, P.; Risqi, A. M.; Prasetio, A.; Ugur, E.; Cao, F.; Imran, I. F.; Said, A. A.; Pininti, A. R.; Subbiah, A. S.; Aydin, E.; Xiao, C.; Seok, S. I.; De Wolf, S. Double-side 2D/3D heterojunctions for inverted perovskite solar cells. *Nature* **2024**, *628* (8006), 93−98.

(2) Yuan, S.; Dai, L.; Sun, Y.; Auras, F.; Zhou, Y.-H.; An, R.-Z.; Liu, Y.; Ding, C.; Cassidy, C.; Tang, X.; Dong, S.-C.; Kang, H.-B.; Chen, K.; Liu, X.; Ye, Z.-F.; Zhao, Y.; Adachi, C.; Liao, L.-S.; Greenham, N. C.; Qi, Y.; Stranks, S. D.; Cui, L.-S.; Friend, R. H. Efficient blue electroluminescence from reduced-dimensional perovskites. *Nat. Photonics* **2024**, *18* (5), 425−431.

(3) Metcalf, I.; Sidhik, S.; Zhang, H.; Agrawal, A.; Persaud, J.; Hou, J.; Even, J.; Mohite, A. D. Synergy of 3D and 2D Perovskites for Durable, Efficient Solar Cells and Beyond. *Chem. Rev.* **2023**, *123* (15), 9565−9652.

(4) Li, X.; Hoffman, J. M.; Kanatzidis, M. G. The 2D Halide Perovskite Rulebook: How the Spacer Influences Everything from the

Structure to Optoelectronic Device Efficiency. *Chem. Rev.* **2021**, *121* (4), 2230−2291.
(5) Tsai, H.; Nie, W.; Blancon, J. C.; Stoumpos, C. C.; Asadpour, R.; Harutyunyan, B.; Neukirch, A. J.; Verduzco, R.; Crochet, J. J.; Tretiak, S.; Pedesseau, L.; Even, J.; Alam, M. A.; Gupta, G.; Lou, J.; Ajayan, P. M.; Bedzyk, M. J.; Kanatzidis, M. G.; Mohite, A. D. High-efficiency two-dimensional Ruddlesden-Popper perovskite solar cells. *Nature* **2016**, *536* (7616), 312−316.
(6) Mao, L.; Stoumpos, C. C.; Kanatzidis, M. G. Two-Dimensional Hybrid Halide Perovskites: Principles and Promises. *J. Am. Chem. Soc.* **2019**, *141* (3), 1171−1190.
(7) Li, X.; Hoffman, J.; Ke, W.; Chen, M.; Tsai, H.; Nie, W.; Mohite, A. D.; Kepenekian, M.; Katan, C.; Even, J.; Wasielewski, M. R.; Stoumpos, C. C.; Kanatzidis, M. G. Two-Dimensional Halide Perovskites Incorporating Straight Chain Symmetric Diammonium Ions, (NH(3)C (m)H(2 m)NH(3))(CH(3)NH(3)) (n-1)Pb (n)I(3 n+1) (m = 4−9; n = 1−4). *J. Am. Chem. Soc.* **2018**, *140* (38), 12226−12238.
(8) Liu, Y.; Zhou, H.; Ni, Y.; Guo, J.; Lu, R.; Li, C.; Guo, X. Revealing stability origin of Dion-Jacobson 2D perovskites with different-rigidity organic cations. *Joule* **2023**, *7* (5), 1016−1032.
(9) Xin, D.; Zhang, M.; Fan, Z.; Yang, Y.; Dong, S.; Lei, L.; Zhao, W.; Lin, Q.; Zheng, X. Low-Dose and Stable X-Ray Imaging Enabled by Low-Dimensional Dion-Jacobson Perovskites. *Adv. Funct. Mater.* **2024**, *34* (38), No. 2402480.
(10) Mandal, A.; Khuntia, S. K.; Mondal, D.; Mahadevan, P.; Bhattacharyya, S. Spin Texture Sensitive Photodetection by Dion-Jacobson Tin Halide Perovskites. *J. Am. Chem. Soc.* **2023**, *145* (45), 24990−25002.
(11) Min, S.; Cho, J. Halide Ion Mobility in Paired 2D Halide Perovskites: Ruddlesden−Popper Versus Dion−Jacobson Phases. *Adv. Opt. Mater.* **2024**, *12* (12), No. 2302516.
(12) Yadav, A.; Vashist, R.; Rahil, M.; Ren, Z.; Yang, Y.; Zhao, B.; Ahmad, S. Smallest Organic Spacers-Based Ruddlesden−Popper and Dion−Jacobson Perovskites: Which One Is Better for Optoelectronics? *J. Phys. Chem. C* **2023**, *127* (45), 22190−22203.
(13) Shang, Y.; Liao, Y.; Wei, Q.; Wang, Z.; Xiang, B.; Ke, Y.; Liu, W.; Ning, Z. Highly stable hybrid perovskite light-emitting diodes based on Dion-Jacobson structure. *Sci. Adv.* **2019**, *5* (8), No. eaaw8072.
(14) Zhang, F.; Park, S. Y.; Yao, C.; Lu, H.; Dunfield, S. P.; Xiao, C.; Ulicna, S.; Zhao, X.; Du Hill, L.; Chen, X.; Wang, X.; Mundt, L. E.; Stone, K. H.; Schelhas, L. T.; Teeter, G.; Parkin, S.; Ratcliff, E. L.; Loo, Y. L.; Berry, J. J.; Beard, M. C.; Yan, Y.; Larson, B. W.; Zhu, K. Metastable Dion-Jacobson 2D structure enables efficient and stable perovskite solar cells. *Science* **2022**, *375* (6576), 71−76.
(15) Zhao, R.; Sabatini, R. P.; Zhu, T.; Wang, S.; Najjarian, A. M.; Johnston, A.; Lough, A. J.; Hoogland, S.; Sargent, E. H.; Seferos, D. S. Rigid Conjugated Diamine Templates for Stable Dion-Jacobson-Type Two-Dimensional Perovskites. *J. Am. Chem. Soc.* **2021**, *143* (47), 19901−19908.
(16) Blancon, J. C.; Stier, A. V.; Tsai, H.; Nie, W.; Stoumpos, C. C.; Traore, B.; Pedesseau, L.; Kepenekian, M.; Katsutani, F.; Noe, G. T.; Kono, J.; Tretiak, S.; Crooker, S. A.; Katan, C.; Kanatzidis, M. G.; Crochet, J. J.; Even, J.; Mohite, A. D. Scaling law for excitons in 2D perovskite quantum wells. *Nat. Commun.* **2018**, *9* (1), No. 2254.
(17) Hansen, K. R.; Wong, C. Y.; McClure, C. E.; Romrell, B.; Flannery, L.; Powell, D.; Garden, K.; Berzansky, A.; Eggleston, M.; King, D. J.; Shirley, C. M.; Beard, M. C.; Nie, W.; Schleife, A.; Colton, J. S.; Whittaker-Brooks, L. Mechanistic origins of excitonic properties in 2D perovskites: Implications for exciton engineering. *Matter* **2023**, *6* (10), 3463−3482.
(18) Tao, W.; Zhang, Y.; Zhu, H. Dynamic Exciton Polaron in Two-Dimensional Lead Halide Perovskites and Implications for Optoelectronic Applications. *Acc. Chem. Res.* **2022**, *55* (3), 345−353.
(19) Tao, W.; Zhang, C.; Zhou, Q.; Zhao, Y.; Zhu, H. Momentarily trapped exciton polaron in two-dimensional lead halide perovskites. *Nat. Commun.* **2021**, *12* (1), No. 1400.
(20) Zhang, H.; Li, W.; Essman, J.; Quarti, C.; Metcalf, I.; Chiang, W.-Y.; Sidhik, S.; Hou, J.; Fehr, A.; Attar, A.; Lin, M.-F.; Britz, A.; Shen, X.; Link, S.; Wang, X.; Bergmann, U.; Kanatzidis, M. G.; Katan, C.; Even, J.; Blancon, J.-C.; Mohite, A. D. Ultrafast relaxation of lattice distortion in two-dimensional perovskites. *Nat. Phys.* **2023**, *19* (4), 545−550.
(21) Thouin, F.; Valverde-Chavez, D. A.; Quarti, C.; Cortecchia, D.; Bargigia, I.; Beljonne, D.; Petrozza, A.; Silva, C.; Kandada, A. R. S. Phonon coherences reveal the polaronic character of excitons in two-dimensional lead halide perovskites. *Nat. Mater.* **2019**, *18* (4), 349−356.
(22) Kandada, A. R. S.; Silva, C. Exciton Polarons in Two-Dimensional Hybrid Metal-Halide Perovskites. *J. Phys. Chem. Lett.* **2020**, *11* (9), 3173−3184.
(23) Righetto, M.; Giovanni, D.; Lim, S. S.; Sum, T. C. The photophysics of Ruddlesden-Popper perovskites: A tale of energy, charges, and spins. *Appl. Phys. Rev.* **2021**, *8* (1), No. 011318.
(24) Fu, J.; Li, M.; Solanki, A.; Xu, Q.; Lekina, Y.; Ramesh, S.; Shen, Z. X.; Sum, T. C. Electronic States Modulation by Coherent Optical Phonons in 2D Halide Perovskites. *Adv. Mater.* **2021**, *33* (11), No. e2006233.
(25) Parra, S. H.; Straus, D. B.; Fichera, B. T.; Iotov, N.; Kagan, C. R.; Kikkawa, J. M. Large Exciton Polaron Formation in 2D Hybrid Perovskites via Time-Resolved Photoluminescence. *ACS Nano* **2022**, *16* (12), 21259−21265.
(26) Sun, Q.; Zhao, C.; Yin, Z.; Wang, S.; Leng, J.; Tian, W.; Jin, S. Ultrafast and High-Yield Polaronic Exciton Dissociation in Two-Dimensional Perovskites. *J. Am. Chem. Soc.* **2021**, *143* (45), 19128−19136.
(27) Bourelle, S. A.; Camargo, F. V. A.; Ghosh, S.; Neumann, T.; van de Goor, T. W. J.; Shivanna, R.; Winkler, T.; Cerullo, G.; Deschler, F. Optical control of exciton spin dynamics in layered metal halide perovskites via polaronic state formation. *Nat. Commun.* **2022**, *13* (1), No. 3320.
(28) Tao, W.; Zhou, Q.; Zhu, H. Dynamic polaronic screening for anomalous exciton spin relaxation in two-dimensional lead halide perovskites. *Sci. Adv.* **2020**, *6* (47), No. eabb7132.
(29) Song, M. S.; Wang, H.; Hu, Z. F.; Zhang, Y. P.; Liu, T. Y.; Wang, H. Y. The Role of Polaronic States on the Spin Dynamics in Solution-Processed Two-Dimensional Layered Perovskite with Different Layer Thickness. *Adv. Sci.* **2023**, *10* (26), No. e2302554.
(30) Zhou, H.; Feng, Q.; Sun, C.; Li, Y.; Tao, W.; Tang, W.; Li, L.; Shi, E.; Nan, G.; Zhu, H. Robust excitonic light emission in 2D tin halide perovskites by weak excited state polaronic effect. *Nat. Commun.* **2024**, *15* (1), No. 8541.
(31) Zhang, Y.; Zhu, L.; Yang, Z.; Tao, W.; Chen, Z.; Li, T.; Lei, H.; Li, C.; Wang, L.; Tian, W.; Li, Z.; Shang, H.; Zhu, H. Transient Photoinduced Pb(2+) Disproportionation for Exciton Self-Trapping and Broadband Emission in Low-Dimensional Lead Halide Perovskites. *J. Am. Chem. Soc.* **2024**, *146* (11), 7831−7838.
(32) Biswas, S.; Zhao, R.; Alowa, F.; Zacharias, M.; Sharifzadeh, S.; Coker, D. F.; Seferos, D. S.; Scholes, G. D. Exciton polaron formation and hot-carrier relaxation in rigid Dion-Jacobson-type two-dimensional perovskites. *Nat. Mater.* **2024**, *23* (7), 937−943.
(33) Stoumpos, C. C.; Cao, D. H.; Clark, D. J.; Young, J.; Rondinelli, J. M.; Jang, J. I.; Hupp, J. T.; Kanatzidis, M. G. Ruddlesden−Popper Hybrid Lead Iodide Perovskite 2D Homologous Semiconductors. *Chem. Mater.* **2016**, *28* (8), 2852−2867.
(34) Ni, L.; Huynh, U.; Cheminal, A.; Thomas, T. H.; Shivanna, R.; Hinrichsen, T. F.; Ahmad, S.; Sadhanala, A.; Rao, A. Real-Time Observation of Exciton-Phonon Coupling Dynamics in Self-Assembled Hybrid Perovskite Quantum Wells. *ACS Nano* **2017**, *11* (11), 10834−10843.
(35) Ziegler, J. D.; Lin, K.-Q.; Meisinger, B.; Zhu, X.; Kober-Czerny, M.; Nayak, P. K.; Vona, C.; Taniguchi, T.; Watanabe, K.; Draxl, C.; Snaith, H. J.; Lupton, J. M.; Egger, D. A.; Chernikov, A. Excitons at the Phase Transition of 2D Hybrid Perovskites. *ACS Photonics* **2022**, *9* (11), 3609−3616.

https://doi.org/10.1021/acsnano.4c12132
ACS Nano 2024, 18, 31485−31494

(36) Chernikov, A.; Berkelbach, T. C.; Hill, H. M.; Rigosi, A.; Li, Y.; Aslan, O. B.; Reichman, D. R.; Hybertsen, M. S.; Heinz, T. F. Exciton binding energy and nonhydrogenic Rydberg series in monolayer WS(2). *Phys. Rev. Lett.* **2014**, *113* (7), No. 076802.
(37) Ye, Z.; Cao, T.; O'Brien, K.; Zhu, H.; Yin, X.; Wang, Y.; Louie, S. G.; Zhang, X. Probing excitonic dark states in single-layer tungsten disulphide. *Nature* **2014**, *513* (7517), 214−218.
(38) Xing, G.; Wu, B.; Wu, X.; Li, M.; Du, B.; Wei, Q.; Guo, J.; Yeow, E. K.; Sum, T. C.; Huang, W. Transcending the slow bimolecular recombination in lead-halide perovskites for electroluminescence. *Nat. Commun.* **2017**, *8* (1), No. 14558.
(39) Simbula, A.; Wu, L.; Pitzalis, F.; Pau, R.; Lai, S.; Liu, F.; Matta, S.; Marongiu, D.; Quochi, F.; Saba, M.; Mura, A.; Bongiovanni, G. Exciton dissociation in 2D layered metal-halide perovskites. *Nat. Commun.* **2023**, *14* (1), No. 4125.
(40) Miyauchi, Y.; Konabe, S.; Wang, F.; Zhang, W.; Hwang, A.; Hasegawa, Y.; Zhou, L.; Mouri, S.; Toh, M.; Eda, G.; Matsuda, K. Evidence for line width and carrier screening effects on excitonic valley relaxation in 2D semiconductors. *Nat. Commun.* **2018**, *9* (1), No. 2598.
(41) Mahmood, F.; Alpichshev, Z.; Lee, Y. H.; Kong, J.; Gedik, N. Observation of Exciton-Exciton Interaction Mediated Valley Depolarization in Monolayer MoSe(2). *Nano Lett.* **2018**, *18* (1), 223−228.
(42) Maialle, M. Z.; de Andrada e Silva, E. A.; Sham, L. J. Exciton spin dynamics in quantum wells. *Phys. Rev. B* **1993**, *47* (23), 15776−15788.
(43) Konabe, S. Screening effects due to carrier doping on valley relaxation in transition metal dichalcogenide monolayers. *Appl. Phys. Lett.* **2016**, *109* (7), No. 073104.
(44) Giovanni, D.; Chong, W. K.; Liu, Y. Y. F.; Dewi, H. A.; Yin, T.; Lekina, Y.; Shen, Z. X.; Mathews, N.; Gan, C. K.; Sum, T. C. Coherent Spin and Quasiparticle Dynamics in Solution-Processed Layered 2D Lead Halide Perovskites. *Adv. Sci.* **2018**, *5* (10), No. 1800664.
(45) Giovanni, D.; Ma, H.; Chua, J.; Gratzel, M.; Ramesh, R.; Mhaisalkar, S.; Mathews, N.; Sum, T. C. Highly spin-polarized carrier dynamics and ultralarge photoinduced magnetization in CH3NH3PbI3 perovskite thin films. *Nano Lett.* **2015**, *15* (3), 1553−1558.
(46) Zhou, H.; Chen, Y.; Zhu, H. Deciphering asymmetric charge transfer at transition metal dichalcogenide-graphene interface by helicity-resolved ultrafast spectroscopy. *Sci. Adv.* **2021**, *7* (34), No. eabg2999, DOI: 10.1126/sciadv.abg2999.
(47) Chen, X.; Lu, H.; Wang, K.; Zhai, Y.; Lunin, V.; Sercel, P. C.; Beard, M. C. Tuning Spin-Polarized Lifetime in Two-Dimensional Metal−Halide Perovskite through Exciton Binding Energy. *J. Am. Chem. Soc.* **2021**, *143* (46), 19438−19445.
(48) Huang, Y.; Chen, C.; Gong, S.; Hu, Q.; Liu, J.; Chen, H.; Mao, L.; Chen, X. Tuning Spin-Polarized Lifetime at High Carrier Density through Deformation Potential in Dion-Jacobson-Phase Perovskites. *J. Am. Chem. Soc.* **2024**, *146* (17), 12225−12232.
(49) Chen, X.; Lu, H.; Li, Z.; Zhai, Y.; Ndione, P. F.; Berry, J. J.; Zhu, K.; Yang, Y.; Beard, M. C. Impact of Layer Thickness on the Charge Carrier and Spin Coherence Lifetime in Two-Dimensional Layered Perovskite Single Crystals. *ACS Energy Lett.* **2018**, *3* (9), 2273−2279.
(50) Guo, Y.; Yaffe, O.; Hull, T. D.; Owen, J. S.; Reichman, D. R.; Brus, L. E. Dynamic emission Stokes shift and liquid-like dielectric solvation of band edge carriers in lead-halide perovskites. *Nat. Commun.* **2019**, *10* (1), No. 1175.
(51) Miyata, K.; Zhu, X. Y. Ferroelectric large polarons. *Nat. Mater.* **2018**, *17* (5), 379−381.
(52) Seiler, H.; Zahn, D.; Taylor, V. C. A.; Bodnarchuk, M. I.; Windsor, Y. W.; Kovalenko, M. V.; Ernstorfer, R. Direct Observation of Ultrafast Lattice Distortions during Exciton-Polaron Formation in Lead Halide Perovskite Nanocrystals. *ACS Nano* **2023**, *17* (3), 1979−1988.
(53) Cannelli, O.; Colonna, N.; Puppin, M.; Rossi, T. C.; Kinschel, D.; Leroy, L. M. D.; Loffler, J.; Budarz, J. M.; March, A. M.; Doumy, G.; Al Haddad, A.; Tu, M. F.; Kumagai, Y.; Walko, D.; Smolentsev, G.; Krieg, F.; Boehme, S. C.; Kovalenko, M. V.; Chergui, M.; Mancini, G. F. Quantifying Photoinduced Polaronic Distortions in Inorganic Lead Halide Perovskite Nanocrystals. *J. Am. Chem. Soc.* **2021**, *143* (24), 9048−9059.
(54) Kashyap, H. K.; Biswas, R. Stokes Shift Dynamics in Ionic Liquids: Temperature Dependence. *J. Phys. Chem. B* **2010**, *114* (50), 16811−16823.
(55) Arzhantsev, S.; Jin, H.; Baker, G. A.; Maroncelli, M. Measurements of the Complete Solvation Response in Ionic Liquids. *J. Phys. Chem. B* **2007**, *111* (18), 4978−4989.
(56) Ullrich, B.; Singh, A. K.; Barik, P.; Xi, H.; Bhowmick, M. Inherent photoluminescence Stokes shift in GaAs. *Opt. Lett.* **2015**, *40* (11), 2580−2583.
(57) Buizza, L. R. V.; Herz, L. M. Polarons and Charge Localization in Metal-Halide Semiconductors for Photovoltaic and Light-Emitting Devices. *Adv. Mater.* **2021**, *33* (24), No. e2007057.
(58) Rudin, S.; Reinecke, T. L.; Segall, B. Temperature-dependent exciton linewidths in semiconductors. *Phys. Rev. B* **1990**, *42* (17), 11218−11231.
(59) Yaffe, O.; Guo, Y.; Tan, L. Z.; Egger, D. A.; Hull, T.; Stoumpos, C. C.; Zheng, F.; Heinz, T. F.; Kronik, L.; Kanatzidis, M. G.; Owen, J. S.; Rappe, A. M.; Pimenta, M. A.; Brus, L. E. Local Polar Fluctuations in Lead Halide Perovskite Crystals. *Phys. Rev. Lett.* **2017**, *118* (13), No. 136001.
(60) Gao, L.; Yadgarov, L.; Sharma, R.; Korobko, R.; McCall, K. M.; Fabini, D. H.; Stoumpos, C. C.; Kanatzidis, M. G.; Rappe, A. M.; Yaffe, O. Metal cation s lone-pairs increase octahedral tilting instabilities in halide perovskites. *Mater. Adv.* **2021**, *2* (14), 4610−4616.
(61) Menahem, M.; Dai, Z.; Aharon, S.; Sharma, R.; Asher, M.; Diskin-Posner, Y.; Korobko, R.; Rappe, A. M.; Yaffe, O. Strongly Anharmonic Octahedral Tilting in Two-Dimensional Hybrid Halide Perovskites. *ACS Nano* **2021**, *15* (6), 10153−10162.
(62) Gu, J.; Tao, Y.; Fu, T.; Guo, S.; Jiang, X.; Guan, Y.; Li, X.; Li, C.; Lu, X.; Fu, Y. Correlating Photophysical Properties with Stereochemical Expression of 6s(2) Lone Pairs in Two-dimensional Lead Halide Perovskites. *Angew. Chem., Int. Ed.* **2023**, *62* (30), No. e202304515.
(63) Amo, Y.; Tominaga, Y. Low-frequency Raman scattering of liquid CCl4, CHCl3, and acetone. *J. Chem. Phys.* **1998**, *109* (10), 3994−3998.
(64) Sharma, R.; Dai, Z.; Gao, L.; Brenner, T. M.; Yadgarov, L.; Zhang, J.; Rakita, Y.; Korobko, R.; Rappe, A. M.; Yaffe, O. Elucidating the atomistic origin of anharmonicity in tetragonal CH3NH3PbI3 with Raman scattering. *Phys. Rev. Mater.* **2020**, *4* (9), No. 092401(R).
(65) Tao, N. J.; Li, G.; Chen, X.; Du, W. M.; Cummins, H. Z. Low-frequency Raman-scattering study of the liquid-glass transition in aqueous lithium chloride solutions. *Phys. Rev. A* **1991**, *44* (10), 6665−6676.
(66) Wu, B.; Wang, A.; Fu, J.; Zhang, Y.; Yang, C.; Gong, Y.; Jiang, C.; Long, M.; Zhou, G.; Yue, S.; Ma, W.; Liu, X. Uncovering the mechanisms of efficient upconversion in two-dimensional perovskites with anti-Stokes shift up to 220 meV. *Sci. Adv.* **2023**, *9* (39), No. eadi9347.
(67) Gong, Y.; Yue, S.; Liang, Y.; Du, W.; Bian, T.; Jiang, C.; Bao, X.; Zhang, S.; Long, M.; Zhou, G.; Yin, J.; Deng, S.; Zhang, Q.; Wu, B.; Liu, X. Boosting exciton mobility approaching Mott-Ioffe-Regel limit in Ruddlesden−Popper perovskites by anchoring the organic cation. *Nat. Commun.* **2024**, *15* (1), No. 1893.